Mixed multiscale finite element methods using approximate global information based on partial upscaling

L. Jiang* Y. Efendiev† I. Mishev‡

November 17, 2008

Abstract

The use of limited global information in multiscale simulations is needed when there is no scale separation. Previous approaches entail fine-scale simulations in the computation of the global information. The computation of the global information is expensive. In this paper, we propose the use of approximate global information based on partial upscaling. A requirement for partial homogenization is to capture long-range (non-local) effects present in the fine-scale solution, while homogenizing some of the smallest scales. The local information at these smallest scales is captured in the computation of basis functions. Thus, the proposed approach allows us to avoid the computations at the scales that can be homogenized. This results to coarser problems for the computation of global fields. We analyze the convergence of the proposed method. Mathematical formalism is introduced which allows estimating the errors due to small scales which are homogenized. The proposed method is applied to simulate two-phase flows in heterogeneous porous media. Numerical results are presented for various permeability fields including those generated using two-point correlation functions and channelized permeability fields from SPE Comparative Project [14]. We consider simple cases where one can identify the scales that can be homogenized. For more general cases, we suggest the use of upscaling on the coarse grid with the size smaller than the target coarse grid where multiscale basis functions are constructed. This intermediate coarse grid renders a partially upscaled solution that contains essential non-local information. Numerical examples demonstrate that the use of approximate global information provides better accuracy than purely local multiscale methods.

1 Introduction

The high degree of variability and multiscale nature of formation properties such as heterogeneous permeability cause significant challenges for subsurface flow modeling. Geological

*IMA, University of Minnesota, Minneapolis, MN 55455. Email: lijiang@ima.umn.edu. Corresponding author

†Department of Mathematics, Texas A&M University, College Station, TX 77843-3368. Email: efendiev@math.tamu.edu

‡Exxonmobil Upstream Research Company, Houston, TX 77252. Email: Ilya.D.Mishev@exxonmobil.com

characterizations that capture these effects are typically developed at scales that are too fine for direct flow simulations. Typically, upscaled or multiscale models are employed for such systems. The main idea of upscaling techniques is to form coarse-scale equations with a prescribed analytical form that may differ from the underlying fine-scale equations. In multiscale methods, the fine-scale information is carried throughout the simulation and the coarse-scale equations are generally not expressed analytically, but rather formed and solved numerically.

In the case of scale separation, one can localize the computation of effective parameters or basis functions. However, these approaches do not perform well if there is no scale separation, and some global information is needed for representing distant/non-local effects. The global information is typically computed on the fine grid and is often computationally expensive. To reduce the computational cost, approximate global information is used in this paper. This becomes particularly helpful if the small scale features dynamically change.

The proposed method uses mixed multiscale finite element method (MsFEM) framework (e.g., [22, 13, 1, 19, 5, 24, 25, 21]). The main idea of MsFEMs is to incorporate the small scale information into finite element basis functions and couple them through a global formulation of the problem. MsFEMs share some similarities with a number of multiscale numerical methods [10, 31, 23]. We remark that special basis functions in finite element methods have been used earlier in [9, 8].

It is known (e.g., [13, 22]) MsFEMs that use only local information suffer from resonance errors. The resonance errors usually exhibit themselves as the ratio between the coarse mesh size and the characteristic length scale. If the mesh size is close to a characteristic length scale, multiscale methods that use only local information may not converge when the ratio between the mesh size and the characteristic length scale is kept fixed. To develop multiscale methods which converge without resonance errors, some limited global information is needed in the construction of basis functions. In the papers [1, 2, 12, 18, 30], limited global information has been successfully used for developing MsFEMs that converge without resonance errors. These methods are applicable for problems without scale separation. Previous approaches involve fine-scale simulations for the computation of global fields that can be computationally expensive.

The use of approximate global fields is not new in multiscale simulations. In [17], the authors compute approximate global fields based on multiscale finite element solutions. This procedure is repeated until convergence. In these simulations, the auxiliary global information is computed iteratively. In this paper, we propose a different approach where limited global information is computed by partial homogenization. Partial homogenization upscales some of the smallest scales that can be captured through local computations of multiscale basis functions (see Figure 1). Such global information can be computed inexpensively and is less sensitive to the changes of the media properties at smallest scales. This is a compromise between local MsFEMs and global MsFEMs where only important non-local information is captured.

In the paper, we use a general framework of the mixed MsFEM with multiple global information following [2]. In [2], the global fields are computed based on fine-scale solutions. It is intuitively clear that the global information needs to contain non-local features of the solution that can not be captured via local solves. We consider a mathematical framework, where the media have both non-separable and separable scales. Separable scales are assumed to be much smaller and, thus, it is desirable to homogenize them. Our objective is to solve the problem on the coarse grid that is larger than the separable scales. As for approximate global fields, we homogenize the media properties over separable scales and compute the global fields on the coarser grid. Detailed analysis for various cases are presented. We consider two scenarios for the scales that are homogenized. In the first case, the scales, which are homogenized, are periodic. For the second case, we use a general G-convergence framework. We show that the mixed MsFEM is stable and the convergence only depends on the small localizable scales, but it is independent of non-local scales.

In the numerical simulations, we introduce an intermediate grid where approximate global fields are computed. This grid size is typically less than the coarse-grid size where multiscale basis functions are constructed. In general, using non-uniform coarsening ([3]) one can reduce the number of coarse grid blocks in the computation of approximate global fields. We would like to note that approximate global fields are pre-computed. The basis functions constructed employing approximate global information can be used to solve flow equations with different source terms, boundary conditions or mobility ($\lambda(x)$ in (1)) on the coarse grid. Moreover, if media properties change at smallest scales that can be localized, one can still use pre-computed approximate global fields.

In the paper, we present some numerical results for various media properties. We consider permeability fields generated using two-point correlation functions ([15]) and channelized permeability fields from SPE Comparative Project [14]. In our numerical results, we use partial upscaling, where the media properties are upscaled to an intermediate coarse grid. Both analytical and numerical upscaling are used depending on the small-scale features that are homogenized. Our numerical results show that one can achieve higher accuracy compared to the local methods when approximate global fields are used.

The paper proceeds as follows. In Section 2, we present mixed MsFEMs that use approximate global fields. Section 3 is devoted to the analysis of the method. Numerical results are presented in Section 4. Finally, some conclusions are made.

2 Mixed MsFEM using approximate global information

2.1 General concept and motivation

In this paper, a mixed MsFEM that uses approximate global (or quasi-global, we may use them interchangeably in the paper) information is studied. First, we briefly motivate the use of global information following [2]. We consider

$$-\, div(\lambda(x)k(x)\nabla p) = f, \tag{1}$$

where $k(x)$ is a heterogeneous field and $\lambda(x)$ is assumed to be a smooth field. This equation is derived from two-phase flow equations when gravity and capillary effects are neglected (see (54)). Here p denotes the pressure. Our goal is to construct multiscale basis functions on the coarse grid (with grid size larger than the characteristic length scales of the problem) such that these basis functions can be used for various source terms $f(x)$, boundary conditions and mobilities $\lambda(x)$. For this reason, one typically looks for functions (local or global) which contain the essential information about the heterogeneities. For problems without scale separation, these functions are often the solutions of global problems, and thus, these methods are effective when Equation (1) is solved multiple times. The underlying assumption for these global fields used in the paper is the following. There exists N global fields p_1,..., p_N (with corresponding velocity fields $u_i = -k\nabla p_i$) and sufficiently smooth scalar functions $A_1(x)$, ..., $A_N(x)$, such that the velocity corresponding to (1) ($u = -\lambda(x)k(x)\nabla p$) can be written as

$$u \approx A_1(x)u_1 + ... + A_N(x)u_N. \tag{2}$$

Note that it is important that A_1, ..., A_N are smooth functions so that the multiscale basis functions which span p_1, ..., p_N (or u_1, ..., u_N) can accurately approximate the global solution. More details on the assumption on A_1, ..., A_N are formulated later. More discussions on the use of global information can be found in [2].

In a general setting, it was shown by Owhadi and Zhang [30] that for an arbitrary smooth $\lambda(x)$, the solution of (1) is a smooth function of d linearly independent solutions of single-phase flow equations ($N = d$), where d is the space dimension. These results are shown under some suitable assumptions for the case $d = 2$ and more restrictive assumptions for the case $d = 3$. In [18], it was shown that for channelized permeability fields, p is a smooth function of single-phase flow pressure (i.e., $N = 1$), where single-phase pressure equation is described by $div(k\nabla p^{sp}) = 0$ with boundary conditions as those corresponding to two-phase flow. Multiple global fields can be used for the system of equations or for the random coefficients.

The computation of global fields is usually expensive. In many applications, the global fields may need to be computed many times depending on changing (dynamic) heterogeneities. For this reason, some type of approximate global fields can be used to speed up the computations. In this paper, we propose multiscale techniques where only essential global information is used in computing basis functions. To obtain this information, we use partial upscaling/homogenization of the fine-scale media properties. The upscaling provides us with a coarse-scale solution which contains essential global information representing the long-range effects. In particular, we use upscaling on coarse grids that are finer than the target coarse grid where multiscale basis functions are computed. In general, one can use non-uniform coarse grids to obtain more accurate global solutions. In Figure 1, we illustrate the concept of partial upscaling. Note that if dynamic changes only affect the small scale features of the permeability which can be captured via local basis functions, our proposed approaches become more effective.

Next, we present an outline of the algorithm which will be presented in a more rigorous mathematical way in Section 2.2. Denote by $\tilde{k}^*$ upscaled permeability field computed on an intermediate coarse grid K_I with the size h_I, where $h_I \leq h$ with h being the coarse grid size where multiscale basis functions are computed. The effective coefficients in upscaling methods are computed using the solution of the local problem in the intermediate coarse grid block (or representative volume). Various boundary conditions can be used for solving the local problems and, for simplicity, we consider

$$div(k(x)\nabla \phi_e) = 0 \text{ in } K_I \tag{3}$$

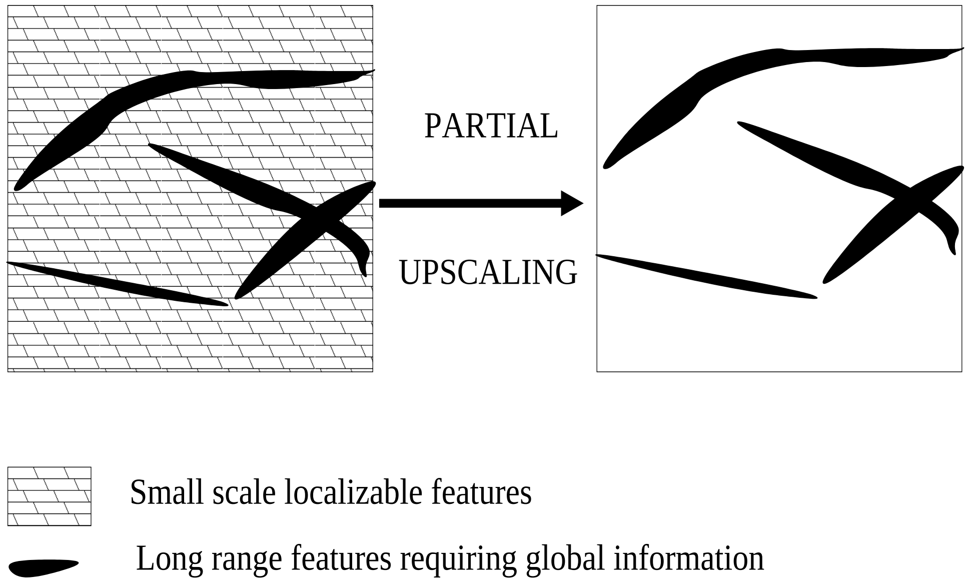

Figure 1: Illustration of partial upscaling.

with $\phi_e(x) = x \cdot e$ on ∂K_I, where e is a unit vector. The effective coefficients are computed in each K_I as

$$\tilde{k^*} e = \frac{1}{|K_I|} \int_{K_I} k \nabla \phi_e dx. \tag{4}$$

We note that $\tilde{k^*}$ (which is not the same as the homogenized coefficients) is a symmetric matrix provided k is symmetric. One can use various boundary conditions, including periodic boundary conditions as well as oversampling methods. We refer to [16, 32] for the discussion on the use of various boundary conditions. Once the effective coefficients are calculated, the coarse-scale equation

$$- div(\tilde{k^*} \nabla p_i^*) = 0 \tag{5}$$

is solved over the entire region to obtain the approximate global fields needed for the computation of multiscale basis functions. In particular, $u_i = -k \nabla p_i^*$ are used as global fields in constructing multiscale basis functions. The index i refers to the global fields and usually obtained by imposing different boundary conditions, e.g., $p_i^* = x_i$ on the global boundary.

Once the global fields are identified, multiscale basis functions are computed by solving the local problems with boundary conditions which depend on p_i^*. For the mixed MsFEM, the basis functions are computed as

$$\begin{aligned} -div(k(x) \nabla \phi_{ij}^K) &= \frac{1}{|K|} \quad \text{in} \quad K \\ -k(x) \nabla \phi_{ij}^K \cdot n_{e_l} &= \delta_{jl} \frac{u_i^* \cdot n_{e_l}}{\int_{e_l} u_i^* \cdot n_{e_l} ds} \quad \text{on} \quad \partial K, \end{aligned}$$

where K is a target coarse grid block and $u_i^* = -\tilde{k}^*(x) \nabla p_i^*$. The basis functions for the solution p is taken to be piece-wise constant functions. Mixed FEM framework is used to couple these basis functions as discussed in the next section.

2.2 Mathematical formalism

In this section, a more rigorous mathematical formalism is presented for the approximate global mixed MsFEM. We introduce ϵ that represent the scales whose effects are homogenized. We denote by $\delta^>$ the scales which are non-separable and have long-range features. The effects of these scales will be captured using global fields. Consider the following elliptic problem with heterogenous coefficients

$$\begin{aligned} -div(k_{\delta^>,\epsilon}(x)\nabla p_{\delta^>,\epsilon}) &= f(x) \quad \text{in} \quad \Omega \\ p_{\delta^>,\epsilon} &= g \quad \text{on} \quad \partial\Omega, \end{aligned} \tag{6}$$

where $k_{\delta^>,\epsilon}(x)$ is a heterogeneous field with two significantly different physical scales $\delta^>$ and ϵ ($\delta^> \gg \epsilon$). Without loss of generality, we assume $k_{\delta^>,\epsilon}$ is symmetric and $\Omega \in \mathbb{R}^2$. Let $u_{\delta^>,\epsilon} = -k_{\delta^>,\epsilon}\nabla p_{\delta^>,\epsilon}$ be the velocity defined in (6).

Let the homogenized equation corresponding to (6) be as following

$$\begin{aligned} -div(k^*_\delta(x)\nabla p^*_\delta) &= f(x) \quad \text{in} \quad \Omega \\ p^*_\delta &= g \quad \text{on} \quad \partial\Omega, \end{aligned} \tag{7}$$

where $k^*_\delta(x)$ is the usual homogenized tensor (defined via periodic homogenization or general $G-$ convergence theory) with parameter δ. We note that the homogenization in (7) is a partial homogenization, i.e., the homogenization is made only for small ϵ scales. Let $u^*_\delta = -k^*_\delta\nabla p^*_\delta$ be the velocity defined in (7). The following assumption (cf. (2)) is used in the analysis.

Assumption A1. There exist functions $u^*_{\delta,1}, \cdots, u^*_{\delta,N}$ and sufficiently smooth $A_1(x), \cdots, A_N(x)$ such that

$$u^*_\delta(x) = \sum_{i=1}^N A_i(x)u^*_{\delta,i}, \quad A_i(x) \in C^\alpha(\Omega), \tag{8}$$

where $u_{\delta,i} = -k^*_\delta\nabla p^*_{\delta,i}$ and $p^*_{\delta,i}$ solves $-div(k^*_\delta(x)\nabla p^*_{\delta,i}) = 0$ in Ω with appropriate boundary conditions.

Remark 2.1. As an example of the *Assumption A1*, we define $u^*_{\delta,i} = -k^*_\delta\nabla p^*_{\delta,i}$ $(i = 1, 2)$ to be solution of the equation

$$\begin{aligned} -div(k^*_\delta\nabla p^*_{\delta,i}) &= 0 \ \text{ in } \ \Omega \\ p^*_{\delta,i} &= x_i \ \text{ on } \ \partial\Omega, \end{aligned} \tag{9}$$

where $x = (x_1, x_2)$. In the harmonic coordinate $(p^*_{\delta,1}, p^*_{\delta,2})$, $p^*_\delta = p^*_\delta(p^*_{\delta,1}, p^*_{\delta,1}) \in W^{2,s}$ $(s \geq 2)$ [30]. Consequently, $u^*_\delta = -k^*_\delta\nabla p^*_\delta = -\sum_{i=1}^2 \frac{\partial p^*_\delta}{\partial p^*_{\delta,i}} k^*_\delta\nabla p^*_{\delta,i} := \sum_{i=1}^2 A_i(x)u^*_{\delta,i}$, where $A_i(x) = \frac{\partial p^*_\delta}{\partial p^*_{\delta,i}} \in W^{1,s}(\Omega)$.

We introduce a quasi-uniform finite element partition τ_h of Ω and let K be a representative coarse element, $h = \max_K \text{diam}_{K\in\tau_h}(K)$. We use the standard notations for Sobolev spaces, and use $\|.\|$ to denote norm, and $|.|$ to denote semi-norm (depending on context, $|.|$ sometimes refers to absolute value). We use multiscale velocity basis functions defined in the following way

$$
\begin{aligned}
-div(k_{\delta>,\epsilon}(x)\nabla\phi_{ij}^K) &= \frac{1}{|K|} \quad \text{in} \quad K \\
-k_{\delta>,\epsilon}(x)\nabla\phi_{ij}^K\cdot n_{e_l} &= \delta_{jl}\frac{u_{\delta,i}^*\cdot n_{e_l}}{\int_{e_l} u_{\delta,i}^*\cdot n_{e_l}ds} \quad \text{on} \quad \partial K \\
\int_K \phi_{ij}^K dx &= 0,
\end{aligned} \tag{10}
$$

where $i=1,...,N$, $j=1,2,3$ (if K is a triangle), e_l is an edge of ∂K, and

$$
\delta_{jj}=1, \quad \delta_{jl}=0 \ \text{ if } \ j\neq l.
$$

Here e_l denotes an edge of K and we omit the subscript e_l in n, if the integral is taken along the edge. Note that for each edge, we have N basis functions and we assume that $u_{\delta,1}^*$,..., $u_{\delta,N}^*$ are linearly independent in order to guarantee that the basis functions are linearly independent. To avoid the possibility that $\int_{e_l} u_{\delta,i}^*\cdot nds$ is zero or unbounded, we make the following assumption for our analysis.

Assumption A2. There exist positive constants C such that

$$
\int_{e_l} |u_{\delta,i}^*\cdot n|ds \leq Ch^{\beta_1} \quad \textit{and} \quad \|\frac{u_{\delta,i}^*\cdot n}{\int_{e_l} u_{\delta,i}^*\cdot nds}\|_{L^r(e_l)} \leq Ch^{-\beta_2+\frac{1}{r}-1}
$$

uniformly for all edges e_l, where $\beta_1\leq 1$, $\beta_2\geq 0$,and $r\geq 1$.

Remark 2.2. The second part of *Assumption A2* is to assure $|\int_{e_l} u_{\delta,i}^*\cdot nds|$ remains positive. If $u_{\delta,i}^*$ are bounded in $L^\infty(e_l)$ for all e_l and $|\int_{e_l} u_{\delta,i}^*\cdot nds|$ remains positive uniformly for all e_l, then $\beta_2=0$. If $|\int_{e_l} u_{\delta,i}^*\cdot nds|\geq Ch^{\beta_1}$ and $\int_{e_l}|u_{\delta,i}^*\cdot n|ds\leq Ch^{\beta_1}$ for all e_l, then we can conclude that $\beta_2=0$ for $r=1$ in *Assumption A2*.

Remark 2.3. If $\int_{e_l} u_{\delta,i}^*\cdot nds$ is zero along some edge e_l, then we can use constant boundary condition in (10) instead, i.e., $\dfrac{u_{\delta,i}^*\cdot n_{e_l}}{\int_{e_l} u_{\delta,i}^*\cdot n_{e_l}ds}$ is replaced by $\frac{1}{|e_l|}$.

We define $\psi_{ij}^K = -k_{\delta>,\epsilon}(x)\nabla\phi_{ij}^K$ and

$$
V_h = \bigoplus_K \{\psi_{ij}^K\} \bigcap H(div,\Omega),
$$

where $H(div,\Omega)=\{v\in L^2(\Omega)|div(v)\in L^2(\Omega)\}$.

The mixed formulation for (6) is to find $\{u_{\delta>,\epsilon},p_{\delta>,\epsilon}\}\in H(div,\Omega)\times L^2(\Omega)$ such that

$$
\begin{aligned}
(k_{\delta>,\epsilon}^{-1}u_{\delta>,\epsilon},v)-(div(v),p) &= -(v\cdot n,g)_{\partial\Omega} \quad \forall v\in H(div,\Omega) \\
-(div(u_{\delta>,\epsilon}),q) &= (f,q) \quad \forall q\in L^2(\Omega),
\end{aligned} \tag{11}
$$

where $(\cdot,\cdot)$ is the usual L^2-inner product. Let $Q_h=\oplus_K P_0(K)\subset L^2(\Omega)$, i.e., piecewise constants, be the basis function space for the pressure. The numerical mixed formulation for (6) is to find $\{u_h,p_h\}\in V_h\times Q_h$ such that and

$$
\begin{aligned}
(k_{\delta>,\epsilon}^{-1}u_h,v_h)-(div(v_h),p_h) &= -(v_h\cdot n,g)_{\partial\Omega} \quad \forall v_h\in V_h \\
-(div(u_h),q_h) &= (f,q_h) \quad \forall q_h\in Q_h.
\end{aligned} \tag{12}
$$

For analysis, we define $\phi_{ij}^{*,K}$ to be the homogenization solution of the basis equation (10), i.e.,

$$\begin{aligned}
-div(k_\delta^*(x)\nabla\phi_{ij}^{*,K}) &= \frac{1}{|K|} \quad \text{in} \quad K \\
-k_\delta^*(x)\nabla\phi_{ij}^{*,K}\cdot n_{e_l} &= \delta_{jl}\frac{u_{\delta,i}^*\cdot n_{e_l}}{\int_{e_l} u_{\delta,i}^*\cdot n_{e_l}ds} \quad \text{on} \quad \partial K \\
\int_K \phi_{ij}^{*,K}dx &= 0.
\end{aligned} \tag{13}$$

We define $\psi_{ij}^{*,K} = -k_\delta^*(x)\nabla\phi_{ij}^{*,K}$ and

$$V_h^* = \bigoplus_K \{\psi_{ij}^{*,K}\}\bigcap H(div,\Omega).$$

We note that V_h^* can be a global multiscale basis space of velocity for equation (7) [2].

Let

$$X = \{u|u = \sum_{i=1}^N a_i(x)u_{\delta,i}^*\}.$$

We define an interpolation operator $\Pi_h^* : X \longrightarrow V_h^*$ such that in each element K, for any $v = \sum_i a_i(x)u_{\delta,i}^* \in X$

$$\Pi_h^*|_K(\sum_i a_i(x)u_{\delta,i}^*) = \sum_{i,j} a_{ij}^K\psi_{ij}^{*,K},$$

where $a_{ij}^K = \int_{e_j} a_i(x)u_{\delta,i}^*\cdot nds.$

3 Convergence analysis

In this section, we present convergence analysis of the method. First, we will prove a stability estimate for the method. Then, we will present the analysis for two cases: when ϵ-scales are periodic; when ϵ-scales are not periodic.

Under some regularity assumptions for $u_{\delta,i}^*$ $(i = 1, \cdots, N)$, we discussed the inf-sup condition in [2] for the multiscale finite element defined in (13) that is only for the homogenized equation (7). For any $q_h \in Q_h$, there exists a constant C^* such that

$$\sup_{v_h\in V_h^*\backslash\{0\}} \frac{\int_\Omega div(v_h)q_h dx}{\|v_h\|_{H(div,\Omega)}} \geq C^*\|q_h\|_{0,\Omega}. \tag{14}$$

Here we assume that (14) holds. Then we can obtain the inf-sup condition for the finite element defined in (10).

Lemma 3.1. *Assume that inequality (14) holds, then for any $q_h \in Q_h$, there exists a constant C such that*

$$\sup_{v_h\in V_h\backslash\{0\}} \frac{\int_\Omega div(v_h)q_h dx}{\|v_h\|_{H(div,\Omega)}} \geq C\|q_h\|_{0,\Omega}. \tag{15}$$

Proof. For any $v_h^* = \sum_{ij} a_{ij}^K \psi_{ij}^{*,K} \in span\{\psi_{ij}^{*,K}\}$, we define $M_K v_h^* = \sum_{ij} a_{ij}^K \psi_{ij}^K \in span\{\psi_{ij}^K\}$. Let $M|_K = M_K$. Then $M : V_h^* \longrightarrow V_h$ is a one to one map. It is easy to check for any $v_h^* \in V_h^*$,

$$div(Mv_h^*) = div(v_h^*) \quad \text{in} \quad K. \tag{16}$$

Let $v_h^* = \sum_{ij} a_{ij}^K \psi_{ij}^{*,K}$ and $z^K = \sum_{ij} \phi_{ij}^K$. Then $M_K v_h^* = -k_{\delta>,\epsilon} \nabla z^K$ and we have

$$\begin{aligned}
&\|M_K v_h^*\|_{0,K}^2 = \int_K k_{\delta>,\epsilon} \nabla z^K \cdot k_{\delta>,\epsilon} \nabla z^K dx \\
&\leq C \int_K k_{\delta>,\epsilon} \nabla z^K \cdot \nabla z^K dx = -C \int_K M_K v_h^* \cdot \nabla z^K dx \\
&= C(\int_K div(M_K v_h^*) z^K dx - \int_{\partial K} (M_K v_h^*) \cdot n z^K ds) \\
&= C(\int_K div(v_h^*) z^K dx - \int_{\partial K} v_h^* \cdot n z^K ds) \\
&= -C \int_K v_h^* \cdot \nabla z^K dx = C \int_K v_h^* \cdot k_{\delta>,\epsilon}^{-1} M_K v_h^* dx \\
&\leq C \|v_h^*\|_{0,K} \|M_K v_h^*\|_{0,K}.
\end{aligned} \tag{17}$$

This yields that $\|M_K v_h^*\|_{0,K} \leq C\|v_h^*\|_{0,K}$. Consequently, combining with (16) implies that for any $v_h^* \in V_h^*$,

$$\|Mv_h^*\|_{H(div,\Omega)} \leq C\|v_h^*\|_{H(div,\Omega)}. \tag{18}$$

Hence, for any $q_h \in Q_h$

$$\begin{aligned}
\sup_{v_h \in V_h \setminus \{0\}} \frac{\int_\Omega div(v_h) q_h dx}{\|v_h\|_{H(div,\Omega)}} &\geq \sup_{v_h^* \in V_h^* \setminus \{0\}} \frac{\int_\Omega div(Mv_h^*) q_h dx}{\|Mv_h^*\|_{H(div,\Omega)}} \\
&\geq \frac{1}{C} \sup_{v_h^* \in V_h^* \setminus \{0\}} \frac{\int_\Omega div(v_h^*) q_h dx}{\|v_h^*\|_{H(div,\Omega)}} \\
&\geq \frac{C^*}{C} \|q_h\|_{0,\Omega},
\end{aligned} \tag{19}$$

where we have used (18) in the second step and (14) in the last step. The proof is complete. □

Because of Lemma 3.1, we use the standard argument (see [11, 13]) and have the following approximation estimate

$$\begin{aligned}
&\|u_{\delta>,\epsilon} - u_h\|_{H(div,\Omega)} + \|p_{\delta>,\epsilon} - p_h\|_{0,\Omega} \\
&\leq C(\inf_{v_h \in V_h} \|u_{\delta>,\epsilon} - v_h\|_{H(div,\Omega)} + \inf_{q_h \in Q_h} \|p_{\delta>,\epsilon} - q_h\|_{0,\Omega}),
\end{aligned} \tag{20}$$

where $\{u_{\delta>,\epsilon}, p_{\delta>,\epsilon}\}$ and $\{u_h, p_h\}$ are the solutions of (11) and (12), respectively.

Let $w_{\delta>,\epsilon}^K(x)$ be the solution of the following equation

$$\begin{aligned}
-div(k_{\delta>,\epsilon}(x) \nabla w_{\delta>,\epsilon}^K) &= div(\Pi_h^* u_\delta^*) \quad \text{in} \quad K \\
-k_{\delta>,\epsilon}(x) \nabla w_{\delta>,\epsilon}^K \cdot n &= \Pi_h^* u_\delta^* \cdot n \quad \text{on} \quad \partial K.
\end{aligned} \tag{21}$$

The homogenized equation of (21) is

$$\begin{aligned} -div(k_\delta^*(x)\nabla w_\delta^{*K}) &= div(\Pi_h^* u_\delta^*) \quad \text{in} \quad K \\ -k_\delta^*(x)\nabla w_\delta^{*K}\cdot n &= \Pi_h^* u_\delta^* \cdot n \quad \text{on} \quad \partial K. \end{aligned} \tag{22}$$

We note *Assumption A1* and define $\Pi_h u_\delta^*|_K := \sum_{ij}(\int_{e_j} A_i u_{\delta,i}^* \cdot nds)\psi_{ij}^K$. Then we have the following lemma.

Lemma 3.2. *Let $w_{\delta>,\epsilon}^K$ and w_δ^{*K} be defined in (21) and (22), respectively. Then*

$$\begin{aligned} -k_{\delta>,\epsilon}(x)\nabla w_{\delta>,\epsilon}^K &= \Pi_h u_\delta^* \quad in \quad K \\ -k_\delta^*(x)\nabla w_\delta^{*K} &= \Pi_h^* u_\delta^* \quad in \quad K. \end{aligned} \tag{23}$$

Proof. By straightforward calculations, it follows that

$$\begin{aligned} div\sum_{ij}(\int_{e_j} A_i u_{\delta,i}^* \cdot nds)(-k_{\delta>,\epsilon}(x)\nabla\phi_{ij}^K) &= div\Pi_h^* u_\delta^* \quad \text{in} \quad K, \\ \sum_{ij}(\int_{e_j} A_i u_{\delta,i}^* \cdot nds)(-k_{\delta>,\epsilon}(x)\nabla\phi_{ij}^K)\cdot n &= \Pi_h^* u_\delta^* \cdot n \quad \text{on} \quad \partial K. \end{aligned} \tag{24}$$

Consequently, Equation (21) and Equation (24) have the same solution up to a constant, which verifies the first equation in the lemma.

By using the same argument as the proof of the first equation in the lemma, we have

$$-k_\delta^*(x)\nabla w_\delta^{*K} = \Pi_h^* u_\delta^*. \tag{25}$$

□

3.1 Convergence analysis for ϵ-periodic case

If the coefficient in (6) is ϵ-periodic, i.e.,

$$k_{\delta>,\epsilon}(x) = k(X_{\delta>}(x), \frac{x}{\epsilon}),$$

where $y \to k(X_{\delta>}(x), y)$ is a Y-periodic function and $X_{\delta>}(x)$ means k has hierarchy of scales (not necessarily separable) larger than δ. In this case, we can compute k_δ^* in the following way. Let $\chi = \{\chi_1, \chi_2\}$ solve the following auxiliary equations,

$$\begin{aligned} -div_y(k(X_{\delta>}(x), y)\nabla\chi_i) &= div_y(k(X_{\delta>}(x), y)e_i) \quad \text{in} \quad Y \\ \langle\chi_i(y)\rangle_Y &= 0. \end{aligned} \tag{26}$$

Here e_i $(i = 1, 2)$ is the unit vector in $\mathbb{R}^2$. Then the homogenized tensor is defined as

$$k_\delta^*(x) = \langle k(\nabla\chi + I)\rangle_Y.$$

We define

$$p_{\delta>,\epsilon}^1 = p_\delta^* + \epsilon\chi\nabla p_\delta^* \quad \text{and} \quad w_{\delta>,\epsilon}^{K,1} = w_\delta^{*K} + \epsilon\chi\nabla w_\delta^{*K}, \tag{27}$$

where p_δ^* and w_δ^{*K} are defined in (7) and in (22), respectively. In the analysis, we use the following assumption.

Assumption A3. $\|\nabla^2 w_\delta^{*K}\|_{0,K} = O(\frac{h}{\delta})$.

Remark 3.1. When $|\nabla k_\delta^*(x)|$ is of order $O(\frac{1}{\delta})$, then classical PDE results (e.g. [20]) imply $\|\nabla^2 w_\delta^{*K}\|_{0,K} = O(\frac{h}{\delta})$ provided that the boundary condition of Equation (22) is sufficiently smooth.

Lemma 3.3. *Suppose Assumptions A1, A2, A3 hold. Let* $p^1_{\delta>,\epsilon}$ *and* $w^{K,1}_{\delta>,\epsilon}$ *be defined as above. Then*

$$|w_\delta^{*K} - p_\delta^*|_{1,K} \leq C(\sum_i \|A_i(x)\|_{C^\alpha(\Omega)})h^{\alpha+\beta_1-\beta_2} \tag{28}$$

$$|w^{K,1}_{\delta>,\epsilon} - p^1_{\delta>,\epsilon}|_{1,K} \leq C(h^{\alpha+\beta_1-\beta_2} + \frac{\epsilon h}{\delta} + \epsilon\|\nabla^2 p_\delta^*\|_{0,K}) \tag{29}$$

$$|w_\delta^{*K}|_{1,\infty,K} \leq C(h^{\alpha+\beta_1-\beta_2-1} + h^{-1}|u_\delta^*|_{0,K} + \|u_\delta^*\|_{0,\infty,K}). \tag{30}$$

Proof. (1). By Lemma 3.2, we have

$$\begin{aligned} |w_\delta^{*K} - p_\delta^*|_{1,K} &= \|(k_\delta^*)^{-1}\Pi_h^* u_\delta^* - (k_\delta^*)^{-1}u_\delta^*\|_{0,K} \\ &\leq C\|\Pi_h^* u_\delta^* - u_\delta^*\|_{0,K} \\ &\leq C(\sum_i \|A_i(x)\|_{C^\alpha(\Omega)})h^{\alpha+\beta_1-\beta_2}, \end{aligned} \tag{31}$$

where we have used Corollary 3.5 from [2].
(2). From the definition $w^{K,1}_{\delta>,\epsilon}$ and $p^1_{\delta>,\epsilon}$, we have

$$\begin{aligned} &|w^{K,1}_{\delta>,\epsilon} - p^1_{\delta>,\epsilon}|_{1,K} \\ &\leq |w_\delta^{*K} - p_\delta^*|_{1,K} + \epsilon\|\nabla_x\chi\nabla(w_\delta^{*K} - p_\delta^*)\|_{0,K} + \epsilon\|\chi(\nabla^2(w_\delta^{*K} - p_\delta^*)\|_{0,K} \\ &\leq Ch^{\alpha+\beta_1-\beta_2} + \epsilon\|\chi\nabla^2 w_\delta^{*K}\|_{0,K} + \epsilon\|\chi\nabla^2 p_\delta^*\|_{0,K} \\ &\leq C(h^{\alpha+\beta_1-\beta_2} + \frac{\epsilon h}{\delta} + \epsilon\|\nabla^2 p_\delta^*\|_{0,K}), \end{aligned} \tag{32}$$

where in the third step we have used *Assumption A3* and the fact that χ and $\nabla\chi$ are bounded in L^∞.

(3). By Lemma 3.2, we have

$$\begin{aligned} |w_\delta^{*K}|_{1,\infty,K} &\leq \|\Pi_h^* u_\delta^* - \langle u_\delta^*\rangle_K\|_{0,\infty,K} + \|\langle u_\delta^*\rangle_K\|_{0,\infty,K} \\ &\leq Ch^{-1}\|\Pi_h^* u_\delta^* - \langle u_\delta^*\rangle_K\|_{0,K} + C\|u_\delta^*\|_{0,\infty,K} \\ &\leq Ch^{-1}\|\Pi_h^* u_\delta^* - u_\delta^*\|_{0,K} + Ch^{-1}\|u_\delta^* - \langle u_\delta^*\rangle_K\|_{0,K} + C\|u_\delta^*\|_{0,\infty,K} \\ &\leq Ch^{\alpha+\beta_1-\beta_2-1} + Ch^{-1}\|u_\delta^*\|_{0,K} + Ch^{-1}\|\langle u_\delta^*\rangle_K\|_{0,K} + C\|u_\delta^*\|_{0,\infty,K} \\ &\leq Ch^{\alpha+\beta_1-\beta_2-1} + Ch^{-1}\|u_\delta^*\|_{0,K} + C\|u_\delta^*\|_{0,\infty,K}, \end{aligned} \tag{33}$$

where we have used the inverse inequality in the second step and Jensen's inequality in last step. ∎

Before we proceed with the convergence analysis, we need the following lemma.

Lemma 3.4. *Let* $p^1_{\delta>,\epsilon}$ *and* $w^{K,1}_{\delta>,\epsilon}$ *be defined in (27). Then*

$$\begin{aligned} |p_{\delta>,\epsilon} - p^1_{\delta>,\epsilon}|_{1,\Omega} &\leq C(\epsilon\|p_\delta^*\|_{2,\Omega} + \sqrt{\epsilon}|p_\delta^*|_{1,\infty,\Omega}) \\ |w^K_{\delta>,\epsilon} - w^{K,1}_{\delta>,\epsilon}|_{1,K} &\leq C(\epsilon\|w_\delta^{*K}\|_{2,K} + \sqrt{\epsilon|\partial K|}|w_\delta^{*K}|_{1,\infty,K}). \end{aligned} \tag{34}$$

The proof of the first estimate in (34) can be referred to [28] and the proof of the second estimate can be referred to Theorem 3.1 in [13].

We have the following convergence theorem.

Theorem 3.5. *Suppose Assumptions A1, A2, A3 hold. Let* $u_{\delta>,\epsilon}$ *and* u_h *solve (11) and (12), respectively. Then*

$$\begin{aligned}
&\|u_{\delta>,\epsilon} - u_h\|_{H(div,\Omega)} + \|p_{\delta>,\epsilon} - p_h\|_{0,\Omega} \\
&\leq C(|p_{\delta>,\epsilon}|_{1,\Omega} + |f|_{1,\Omega})h + C(\epsilon\|p_\delta^*\|_{2,\Omega} + \sqrt{\epsilon}|p_\delta^*|_{1,\infty,\Omega}) \\
&+ C\frac{\epsilon}{\delta} + Ch^{\alpha+\beta_1-\beta_2-1} + C(\|u_\delta^*\|_{0,\Omega} + \|u_\delta^*\|_{0,\infty,\Omega})\sqrt{\frac{\epsilon}{h}}.
\end{aligned} \tag{35}$$

Proof. For the proof, it suffices to choose a proper q_h and v_h such that the right hand side of (20) is small. Set $q_h|_K = \langle p_{\delta>,\epsilon}\rangle_K$. Then Poincaré-Friedrichs inequality implies

$$\inf_{q_h\in Q_h} \|p_{\delta>,\epsilon} - p_h\|_{0,\Omega} \leq Ch|p_{\delta>,\epsilon}|_{1,\Omega}. \tag{36}$$

We choose $v_h = \sum_{i,j} c_{ij}^K \psi_{ij}^K = \Pi_h u_\delta^*$ in K on the right hand side of (20). Because

$$\int_K \sum_i div(A_i(x)u_{\delta,i}^*)dx = f,$$

we get by the divergence theorem

$$\int_{\partial K} \sum_i A_i(x)u_{\delta,i}^* \cdot n ds = f.$$

This gives rise to

$$\begin{aligned}
\|div(u_{\delta>,\epsilon} - \sum_{i,j} c_{ij}^K \psi_{ij}^K)\|_{0,K} &= \|f - \sum_{i,j} c_{ij}^K \frac{1}{|K|}\|_{0,K} \\
&= \|f - \sum_{i,j} \int_{e_j} A_i(x)u_{\delta,i}^* \cdot n ds \frac{1}{|K|}\|_{0,K} \\
&= \|f - \langle f\rangle_K\|_{0,K} \\
&\leq Ch|f|_{1,K}.
\end{aligned} \tag{37}$$

After making the summation over all K for (37), we have

$$\|div(u_{\delta>,\epsilon} - v_h)\|_{0,\Omega} \leq Ch|f|_{1,\Omega}. \tag{38}$$

Now we apply Lemma 3.3 to estimate $\|u_{\delta>,\epsilon} - v_h\|_{0,K}$:

$$
\begin{aligned}
&\|u_{\delta>,\epsilon} - v_h\|_{0,K} \\
&= \|k_{\delta>,\epsilon}\nabla p_{\delta>,\epsilon} - k_{\delta>,\epsilon}\nabla w^K_{\delta>,\epsilon}\|_{0,K} \\
&\le C\|\nabla p_{\delta>,\epsilon} - \nabla w^K_{\delta>,\epsilon}\|_{0,K} \\
&\le C\|\nabla p_{\delta>,\epsilon} - \nabla p^1_{\delta>,\epsilon}\|_{0,K} + C\|\nabla p^1_{\delta>,\epsilon} - \nabla w^{K,1}_{\delta>,\epsilon}\|_{0,K} + C\|\nabla w^{K,1}_{\delta>,\epsilon} - \nabla w^K_{\delta>,\epsilon}\|_{0,K} \\
&\le C\|\nabla p_{\delta>,\epsilon} - \nabla p^1_{\delta>,\epsilon}\|_{0,K} + C(h^{\alpha+\beta_1-\beta_2} + \frac{\epsilon h}{\delta} + \epsilon\|\nabla^2 p^*_\delta\|_{0,K}) \\
&+ C(\epsilon\|w^{*K}_\delta\|_{2,K} + \sqrt{\epsilon|\partial K|}|w^{*K}_\delta|_{1,\infty,K}) \\
&\le C\|\nabla p_{\delta>,\epsilon} - \nabla p^1_{\delta>,\epsilon}\|_{0,K} + C(h^{\alpha+\beta_1-\beta_2} + \frac{\epsilon h}{\delta} + \epsilon\|\nabla^2 p^*_\delta\|_{0,K}) \\
&+ C[\frac{\epsilon h}{\delta} + \sqrt{\epsilon|\partial K|}(h^{\alpha+\beta_1-\beta_2-1} + h^{-1}\|u^*_\delta\|_{0,K} + \|u^*_\delta\|_{0,\infty,K})].
\end{aligned}
\tag{39}
$$

Making the summation all over K, we have

$$
\begin{aligned}
&\|u_{\delta>,\epsilon} - v_h\|_{0,\Omega} \\
&\le C\|\nabla p_{\delta>,\epsilon} - \nabla p^1_{\delta>,\epsilon}\|_{0,\Omega} + C\frac{\epsilon}{\delta} + C(h^{\alpha+\beta_1-\beta_2-1} + \sqrt{\frac{\epsilon}{h}}h^{\alpha+\beta_1-\beta_2-1}) \\
&+ C\epsilon\|\nabla^2 p^*_\delta\|_{0,K} + C\sqrt{\frac{\epsilon}{h}}\|u^*_\delta\|_{0,\Omega} + C\sqrt{\frac{\epsilon}{h}}\|u^*_\delta\|_{0,\infty,\Omega} \\
&\le C(\epsilon\|p^*_\delta\|_{2,\Omega} + \sqrt{\epsilon}|p^*_\delta|_{1,\infty,\Omega}) + C\frac{\epsilon}{\delta} + Ch^{\alpha+\beta_1-\beta_2-1} + C(\|u^*_\delta\|_{0,\Omega} + \|u^*_\delta\|_{0,\infty,\Omega})\sqrt{\frac{\epsilon}{h}}.
\end{aligned}
\tag{40}
$$

Therefore, invoking (20), (36), (38) and (40), we have

$$
\begin{aligned}
&\|u_{\delta>,\epsilon} - u_h\|_{H(div,\Omega)} + \|p_{\delta>,\epsilon} - p_h\|_{0,\Omega} \\
&\le C(|p_{\delta>,\epsilon}|_{1,\Omega} + |f|_{1,\Omega})h + C(\epsilon\|p^*_\delta\|_{2,\Omega} + \sqrt{\epsilon}|p^*_\delta|_{1,\infty,\Omega}) \\
&+ C\frac{\epsilon}{\delta} + Ch^{\alpha+\beta_1-\beta_2-1} + C(\|u^*_\delta\|_{0,\Omega} + \|u^*_\delta\|_{0,\infty,\Omega})\sqrt{\frac{\epsilon}{h}}.
\end{aligned}
\tag{41}
$$

This completes the proof. □

Remark 3.2. The term $\sqrt{\frac{\epsilon}{h}}$ comes from the partial homogenization with respect to ϵ-scales. If we use the local mixed MsFEM (i.e., boundary conditions for velocity basis equations are constants), then the proof in [13] implies that the convergence rate in Theorem 3.5 would contain the term $\sqrt{\frac{\delta}{h}}$ (if $k_{\delta>,\epsilon}$ is also δ-periodic), which is larger than $\sqrt{\frac{\epsilon}{h}}$. This is an accuracy improvement of the approximate global mixed MsFEM compared to the local mixed MsFEM.

Instead of *Assumption A3*, the following alternative assumption can be used.

Assumption A3'. $|(\Pi_h - I)u^*_\delta|_{1,\Omega} \le C\|u^*_\delta\|_{1,\Omega}$ *for the velocity* u^*_δ.

Under *Assumption A3'*, we have the following proposition.

Proposition 3.6. *Suppose Assumption A1, A2, A3' hold. Let $u_{\delta>,\epsilon}$ and u_h solve the equation (11) and (12), respectively. Then*

$$\begin{aligned}&\|u_{\delta>,\epsilon}-u_h\|_{H(div,\Omega)}+\|p_{\delta>,\epsilon}-p_h\|_{0,\Omega}\\&\le C(|p_{\delta>,\epsilon}|_{1,\Omega}+|f|_{1,\Omega})h+C(\|p^*_\delta\|_{2,\Omega}+\|u^*_\delta\|_{1,\Omega})\epsilon+C\sqrt{\epsilon}|p^*_\delta|_{1,\infty,\Omega}\\&+Ch^{\alpha+\beta_1-\beta_2-1}+C(\|u^*_\delta\|_{0,\Omega}+\|u^*_\delta\|_{0,\infty,\Omega})\sqrt{\frac{\epsilon}{h}}.\end{aligned} \tag{42}$$

Proof. First, we can show the following estimate under *Assumption A3'*:

$$\begin{aligned}&|w^{K,1}_{\delta>,\epsilon}-p^1_{\delta>,\epsilon}|_{1,K}\\&\le|w^{*K}_\delta-p^*_\delta|_{1,K}+\epsilon\|\nabla_x\chi\nabla(w^{*K}_\delta-p^*_\delta)\|_{0,K}+\epsilon\|\chi(\nabla^2(w^{*K}_\delta-p^*_\delta)\|_{0,K}\\&\le Ch^{\alpha+\beta_1-\beta_2}+\epsilon\|\nabla((k^*_\delta)^{-1}\Pi^*_hu^*_\delta-(k^*_\delta)^{-1}u^*_\delta)\|_{0,K}\\&\le Ch^{\alpha+\beta_1-\beta_2}+\epsilon\|(\nabla(k^*_\delta)^{-1})\cdot(\Pi^*_hu^*_\delta-u^*_\delta)\|_{0,K}+\epsilon\|(k^*_\delta)^{-1}\nabla(\Pi^*_hu^*_\delta-u^*_\delta)\|_{0,K}\\&\le Ch^{\alpha+\beta_1-\beta_2}+C\frac{\epsilon}{\delta}h^{\alpha+\beta_1-\beta_2}+C\epsilon\|u^*_\delta\|_{1,K},\end{aligned} \tag{43}$$

where "$\cdot$" in the third step is the tensor dot product. Here we have used the assumption $|\nabla(k^*_\delta)^{-1}|=O(\frac{1}{\delta})$. By the estimate (43) and Lemma 3.2, we have

$$\begin{aligned}&\|u_{\delta>,\epsilon}-v_h\|_{0,K}\\&\le C\|\nabla p_{\delta>,\epsilon}-\nabla w^K_{\delta>,\epsilon}\|_{0,K}\\&\le C\|\nabla p_{\delta>,\epsilon}-\nabla p^1_{\delta>,\epsilon}\|_{0,K}+C\|\nabla p^1_{\delta>,\epsilon}-\nabla w^{K,1}_{\delta>,\epsilon}\|_{0,K}+C\|\nabla w^{K,1}_{\delta>,\epsilon}-\nabla w^K_{\delta>,\epsilon}\|_{0,K}\\&\le C\|\nabla p_{\delta>,\epsilon}-\nabla p^1_{\delta>,\epsilon}\|_{0,K}+C(h^{\alpha+\beta_1-\beta_2}+\epsilon\|u^*_\delta\|_{1,K})+C(\epsilon\|w^{*K}_\delta\|_{2,K}+\sqrt{\epsilon|\partial K|}|w^{*K}_\delta|_{1,\infty,K})\\&\le C\|\nabla p_{\delta>,\epsilon}-\nabla p^1_{\delta>,\epsilon}\|_{0,K}+C(h^{\alpha+\beta_1-\beta_2}+\epsilon\|u^*_\delta\|_{1,K})\\&+C[\epsilon\|u^*_\delta\|_{1,K}+\sqrt{\epsilon|\partial K|}(h^{\alpha+\beta_1-\beta_2-1}+h^{-1}\|u^*_\delta\|_{0,K}+\|u^*_\delta\|_{0,\infty,K})].\end{aligned} \tag{44}$$

The rest of the proof follows the proof of Theorem 3.5. □

Corollary 3.7. *Let k^*_δ has periodicity with period δ and $|p^*_\delta|_{L^\infty(\Omega)}\le C$. If the boundary condition $g\in C^{1,\nu}(\partial\Omega)$ $(\nu>0)$ in (7), then*

$$\begin{aligned}&\|u_{\delta>,\epsilon}-u_h\|_{H(div,\Omega)}+\|p_{\delta>,\epsilon}-p_h\|_{0,\Omega}\\&\le C(h^{\min(1,\alpha+\beta_1-\beta_2-1)}+\frac{\epsilon}{\delta}+\sqrt{\frac{\epsilon}{h}}).\end{aligned} \tag{45}$$

Proof. If k^*_δ is $\delta-$periodic, then the asymptotic expansion for p^*_δ implies that

$$\|p^*_\delta\|_{2,\Omega}\le C\delta^{-1}.$$

Moreover, if the boundary condition $g\in C^{1,\nu}(\partial\Omega)$, Lemma 20 in [7] implies that for any K

$$\|\nabla p^*_\delta\|_{L^\infty(K)}\le C.$$

Consequently, (45) follows immediately by the proof of Theorem 3.5. □

In the proof of (33), if we use Poincaré-Friedrichs inequality in the third step, then we obtain that

$$|w_\delta^{*K}|_{1,\infty,K} \le C(h^{\alpha+\beta_1-\beta_2-1} + C\|u_\delta^*\|_{1,K} + C\|u_\delta^*\|_{0,\infty,K}). \tag{46}$$

Using the estimate (46) and the proof of Theorem 3.5, we have

$$\begin{aligned} &\|u_{\delta>,\epsilon} - u_h\|_{H(div,\Omega)} + \|p_{\delta>,\epsilon} - p_h\|_{0,\Omega} \\ &\le C(|p_{\delta>,\epsilon}|_{1,\Omega} + |f|_{1,\Omega})h + C(\epsilon\|p_\delta^*\|_{2,\Omega} + \sqrt{\epsilon}|p_\delta^*|_{1,\infty,\Omega}) \\ &+ C\frac{\epsilon}{\delta} + Ch^{\alpha+\beta_1-\beta_2-1} + C\|u_\delta^*\|_{1,\Omega}\sqrt{\epsilon h} + C\|u_\delta^*\|_{0,\infty,\Omega}\sqrt{\frac{\epsilon}{h}}. \end{aligned} \tag{47}$$

We note the resonance error term $\sqrt{\frac{\epsilon}{h}}$ (as $\epsilon \approx h$) in the estimate (47). Actually, this resonance error term comes from the term $|w_\delta^{*K}|_{1,\infty,K}$ in (39).

Remark 3.3. The mixed MsFEM presented here is an extension of Chen and Hou's mixed MsFEM proposed in [13] and of the global mixed MsFEM proposed in [2]. If we choose only one global field $u_{\delta,1}^*$ in *Assumption A1* and set $u_{\delta,1}^*$ to be constant field globally or in $span\{R_j^K\}$ locally, where R_j^K is a lowest Raviart-Thomas finite element basis function, then the method presented in the paper reduces to the local method in [13]. If $k_{\delta>,\epsilon}(x)$ does not have ϵ-scale, then the method in the paper is the global method presented in [2] and the convergence rate depends on coarse mesh size h only.

Remark 3.4. We note there is a resonance error $O(\sqrt{\frac{\epsilon}{h}})$ in Theorem 3.5 (or the estimate (47)). This is because we have only used the homogenization information about ϵ-scale in (10) when we construct multiscale velocity basis functions. In order to remove this resonance error, we can use the global mixed MsFEM [2], but this will be computationally expensive.

Remark 3.5. The basis functions in (10) define a conforming mixed MsFEM. If the equation (10) is solved in block S larger than K and the interior information of ψ_{ij}^S is taken to construct the basis functions in K, then this is the oversampling technique introduced in [13]. Following the outline in [13] and using the estimate (46), we can obtain the following convergence estimate

$$\begin{aligned} &\|u_{\delta>,\epsilon} - u_h\|_{H(div,\Omega)} + \|p_{\delta>,\epsilon} - p_h\|_{0,\Omega} \\ &\le C(|p_{\delta>,\epsilon}|_{1,\Omega} + |f|_{1,\Omega})h + C\epsilon\|p_\delta^*\|_{2,\Omega} + C\frac{\epsilon}{\delta} \\ &+ C|u_\delta^*|_{1,\Omega}\sqrt{\epsilon h} + Ch^{\alpha+\beta_1-\beta_2-1} + C(\frac{\epsilon}{h} + \sqrt{\epsilon})\|u_\delta^*\|_{0,\infty,\Omega}. \end{aligned} \tag{48}$$

Consequently, the resonance error $O(\sqrt{\frac{\epsilon}{h}})$ in Theorem 3.5 reduces to $O(\frac{\epsilon}{h})$.

Remark 3.6. If there is strong scale separation, one can use smaller regions (smaller than K) to construct multiscale basis functions.

3.2 Convergence analysis in $G-$convergence

In Section 3.1, we investigated the case when $k_{\delta>,\epsilon}$ in (6) is ϵ periodic. However, the mixed MsFEM defined in (10) can be applied to non-periodic problems. In this section we will discuss the convergence for non-periodic case within the framework $G-$convergence theory (e.g. [26]).

A sequence of matrices $k_{\delta>,\epsilon}$ ($k_{\delta>,\epsilon}$ is symmetric and δ scale is fixed) is $G-$convergent to k_δ^* if for any open set $\omega \subset \Omega$ and any right hand side $f \in H^{-1}(\omega)$ in (6), if the sequence of the solutions $p_{\delta>,\epsilon}$ in (6) satisfies

$$p_{\delta>,\epsilon} \rightharpoonup p_\delta^* \text{ weakly in } H^1(\omega) \text{ as } \epsilon \to 0,$$

where p_δ^* is the solution of the equation (7), in which k_δ^* is the homogenized matrix in the sense of $G-$convergence. The $G-$convergence implies that

$$k_{\delta>,\epsilon}\nabla p_{\delta>,\epsilon} \rightharpoonup k_\delta^*\nabla p_\delta^* \text{ weakly in } L^2(\omega) \text{ as } \epsilon \to 0.$$

There is no explicit formula for the matrix k_δ^*, which is defined as a limit in the distributional sense, i.e.,

$$k_{\delta>,\epsilon}\nabla N^i_{\delta>,\epsilon} \rightharpoonup k_\delta^* e_i \text{ in } \mathcal{D}'(\omega;\mathbb{R}^2),$$

where the auxiliary functions $N^i_{\delta>,\epsilon}$ $(i = 1, 2)$ satisfy

$$N^i_{\delta>,\epsilon} \rightharpoonup x_i \text{ weakly in } H^1(\omega) \text{ as } \epsilon \to 0.$$

The auxiliary functions are not explicit. They are unique up to an additional sequence converging strongly to 0 in $H^1(\omega)$. As an option, we can define them as the solution of the following equation

$$\begin{aligned} -div(k_{\delta>,\epsilon}\nabla N^i_{\delta>,\epsilon}) &= -div(k_\delta^* e_i) \text{ in } \omega \\ N^i_{\delta>,\epsilon} &= x_i \text{ on } \partial\omega. \end{aligned} \tag{49}$$

We define the corrector matrix $\nabla N_{\delta>,\epsilon} = (\frac{\partial N^i_{\delta>,\epsilon}}{\partial x_j})_{i,j=1,2}$. Then, we have the following lemma.

Lemma 3.8. *[29] Let $k_{\delta>,\epsilon}$ be a sequence $G-$converging to k_δ^* as $\epsilon \to 0$. Then*

$$\nabla p_{\delta>,\epsilon} = \nabla N_{\delta>,\epsilon} \cdot \nabla p_\delta^* + R^\omega_{\delta>,\epsilon},$$

where $R^\omega_{\delta>,\epsilon} \to 0$ strongly in $L^1(\omega)$ as $\epsilon \to 0$. Moreover, if $\nabla N_{\delta>,\epsilon}$ is bounded in $L^r(\omega)$ for some r such that $2 \le r \le \infty$, and $\nabla p_\delta^* \in L^s(\omega)$ for some s such that $2 \le s < \infty$, then $R^\omega_{\delta>,\epsilon} \to 0$ strongly in $L^t(\omega)$, as $\epsilon \to 0$, where $t = \min\{2, \frac{rs}{r+s}\}$.

Theorem 3.9. *Suppose Assumptions A1 and A2 hold. Let $u_{\delta>,\epsilon}$ and u_h solve (11) and (12), respectively. If $\nabla N_{\delta>,\epsilon} \in L^\infty(K)$ for any K and $p_\delta^* \in H^1(\Omega)$, then*

$$\lim_{h\to 0}\lim_{\epsilon\to 0}(\|u_{\delta>,\epsilon} - u_h\|_{H(div,\Omega)} + \|p_{\delta>,\epsilon} - p_h\|_{0,\Omega}) = 0. \tag{50}$$

Proof. Let v_h and q_h be defined as the same as in the proof of Theorem 3.5. We have

$$\|div(u_{\delta>,\epsilon} - v_h)\|_{0,\Omega} + \|p_{\delta>,\epsilon} - q_h\|_{0,\Omega} \le Ch(|p_{\delta>,\epsilon}|_{1,\Omega} + |f|_{1,\Omega}).$$

Now we apply Lemma 3.8 to estimate $\|u_{\delta>,\epsilon} - v_h\|_{0,K}$:

$$
\begin{aligned}
&\|u_{\delta>,\epsilon} - v_h\|_{0,K} \\
&= \|k_{\delta>,\epsilon}\nabla p_{\delta>,\epsilon} - k_{\delta>,\epsilon}\nabla w^K_{\delta>,\epsilon}\|_{0,K} \\
&\leq C\|\nabla p_{\delta>,\epsilon} - \nabla w^K_{\delta>,\epsilon}\|_{0,K} \\
&\leq C\|\nabla p_{\delta>,\epsilon} - \nabla N_{\delta>,\epsilon}\cdot\nabla p^*_\delta\|_{0,K} + C\|\nabla N_{\delta>,\epsilon}\cdot(\nabla p^*_\delta - \nabla w^{*K}_\delta)\|_{0,K} \\
&+ C\|\nabla N_{\delta>,\epsilon}\cdot\nabla w^{*K}_\delta - \nabla w^K_{\delta>,\epsilon}\|_{0,K} \\
&\leq C\|\nabla p_{\delta>,\epsilon} - \nabla N_{\delta>,\epsilon}\cdot\nabla p^*_\delta\|_{0,K} + Ch^{\alpha+\beta_1-\beta_2} + C\|R^K_{\delta>,\epsilon}\|_{0,K}.
\end{aligned}
\tag{51}
$$

Let $\nabla p^1_{\delta>,\epsilon} = \nabla N_{\delta>,\epsilon}\cdot\nabla p^*_\delta$. Making the summation all over K, we have

$$
\begin{aligned}
&\|u_{\delta>,\epsilon} - v_h\|_{0,\Omega} \\
&\leq C\|\nabla p_{\delta>,\epsilon} - \nabla p^1_{\delta>,\epsilon}\|_{0,\Omega} + Ch^{\alpha+\beta_1-\beta_2-1} + C\sum_K \|R^K_{\delta>,\epsilon}\|_{0,K} \\
&\leq C\|R^\Omega_{\delta>,\epsilon}\|_{0,\Omega} + Ch^{\alpha+\beta_1-\beta_2-1} + C\sum_K \|R^K_{\delta>,\epsilon}\|_{0,K}.
\end{aligned}
\tag{52}
$$

Consequently, we have by (20)

$$
\begin{aligned}
&\|u_{\delta>,\epsilon} - u_h)\|_{H(div,\Omega)} + \|p_{\delta>,\epsilon} - p_h\|_{0,\Omega} \\
&\leq Ch(|p_{\delta>,\epsilon}|_{1,\Omega} + |f|_{1,\Omega}) + C\|R^\Omega_{\delta>,\epsilon}\|_{0,\Omega} + Ch^{\alpha+\beta_1-\beta_2-1} + C\sum_K \|R^K_{\delta>,\epsilon}\|_{0,K}.
\end{aligned}
\tag{53}
$$

The proof is completed by taking $\epsilon \to 0$, $h \to 0$ and applying Lemma 3.8. □

Remark 3.7. From Lemma 3.8, it follows that in any open set $\omega \subset \Omega$

$$u_{\delta>,\epsilon} \approx k_{\delta>,\epsilon}\nabla N_{\delta>,\epsilon}\cdot\nabla p^*_\delta \ \text{ in } \ L^2(\omega),$$

for sufficiently small ϵ. This is the motivation of the mixed MsFEM proposed in [2] for the $G-$convergence homogenization case.

By Theorem 2.4 in [4], we can obtain the following result.

Proposition 3.10. *Let the $G-$limit $p^*_\delta \in W^{2,\infty}(\Omega)$ and $N_{\delta>,\epsilon} = \{N^1_{\delta>,\epsilon}, N^2_{\delta>,\epsilon}\}$ be uniformly bounded in $L^q(\Omega)$ for any $2 \leq q < \infty$. Then*

$$\lim_{\epsilon\to 0}\|u_{\delta>,\epsilon} - k_{\delta>,\epsilon}\nabla N_{\delta>,\epsilon}\cdot(\nabla p^*_\delta)\circ N_{\delta>,\epsilon}\|_{0,\Omega} = 0,$$

where $\circ$ denotes the composition of functions.

Remark 3.8. $u_{\delta>,\epsilon} \approx k_{\delta>,\epsilon}\nabla N_{\delta>,\epsilon}\cdot(\nabla p^*_\delta)\circ N_{\delta>,\epsilon}$ in $L^2(\Omega)$ implies that approximate global fields can be used in (2) (or *Assumption A1*).

Remark 3.9. Since k^*_δ is not explicit when $k_{\delta>,\epsilon}$ is not $\epsilon-$periodic, we can not solve $N^i_{\delta>,\epsilon}$ in (49) and $p^*_{\delta,i}$ in *Assumption A1* directly. However, we can use upscaling method to obtain an upscaled $\tilde{k}^*_\delta$ in coarse block, which is approximated to k^*_δ.

4 Numerical results

In this section, we present numerical results for permeability fields from SPE Comparative Solution Project [14] (also known as SPE 10) and two point correlation permeability fields [15]. Because of channelized structure of SPE 10 permeability fields, the localized approaches do not perform well. We will show that if one uses an approximate global field based on single-phase flow information in constructing multiscale basis functions, then the numerical approximation on the coarse grid becomes more accurate.

In our numerical simulations, we will perform two-phase flow and transport simulations. The equations are given (in the absence of gravity and capillary effects) by flow equations

$$div(\lambda(S)k\nabla p) = f, \tag{54}$$

where the total mobility $\lambda(S)$ is given by $\lambda(S) = \lambda_w(S) + \lambda_o(S)$ and f is a source term. Here, $\lambda_w(S) = k_{rw}(S)/\mu_w$ and $\lambda_o(S) = k_{ro}(S)/\mu_o$ where μ_o and μ_w are viscosities of oil and water phases, correspondingly, and $k_{rw}(S)$ and $k_{ro}(S)$ are relative permeabilities of oil and water phases, correspondingly. The saturation is governed by

$$\frac{\partial S}{\partial t} + div(F) = 0, \tag{55}$$

where $F = vf_w(S)$, with $f_w(S)$, the fractional flow of water, given by $f_w = \lambda_w/(\lambda_w + \lambda_o)$, and the total velocity v by:

$$v = v_w + v_o = -\lambda(S)k\nabla p. \tag{56}$$

In our simulations, we take $k_{rw}(S) = S^2$ and $k_{ro}(S) = (1-S)^2$. In the presence of capillary effects, an additional diffusion term is present in (55). In the simulations, we solve the pressure equation on the coarse grid and re-construct the fine-scale velocity field which is used to solve the saturation equation. The basis functions are constructed at time zero and not changed throughout the simulations.

We compare the saturation fields and water-cut data as a function of pore volume injected (PVI). The water-cut is defined as the fraction of water in the produced fluid and is given by q_w/q_t, where $q_t = q_o + q_w$, with q_o and q_w being the flow rates of oil and water at the production edge of the model. In particular, $q_w = \int_{\partial\Omega^{out}} f(S)v \cdot n ds$, $q_t = \int_{\partial\Omega^{out}} v \cdot n ds$, where $\partial\Omega^{out}$ is the outer flow boundary. Pore volume injected, defined as $PVI = \frac{1}{V_p}\int_0^t q_t(\tau)d\tau$, with V_p being the total pore volume of the system, provides the dimensionless time for the displacement. We consider a traditional quarter five-spot problem (e.g., [1]), where the water is injected at left left top corner and oil is produced at the right lower corner of the rectangular domain. In all numerical simulations, mixed multiscale basis functions are constructed once at the beginning of the computations. In the discussions, we refer to the grid where multiscale basis functions are constructed as a coarse grid, and to the grid that is used to compute global fields as an upscaling grid.

For our first numerical example, we choose $k_{\delta>,\epsilon} = k_\delta k_\epsilon$, where k_δ is (volume) averaged SPE 10 permeability (layer 60) on 50×50 grid (uniform in each direction), and k_ϵ is a checkerboard permeability with values 10 or 1 on the fine grid, 300×300. We depict the fine-scale (300×300) permeability $k_{\delta>,\epsilon}$ and the homogenized permeability k_δ^* of $k_{\delta>,\epsilon}$ on 50×50 in Figure 2. Note that the homogenization does not affect k_δ and the homogenized permeability is $k_\delta^* = \sqrt{10}k_\delta$ (see the bottom plot in Figure 2). This example is suitable to the analysis presented in Section 2.2. In particular, the partial homogenization (homogenization with respect to ϵ only) can be computed analytically. Figure 3 depicts the reference (fine-scale) saturation, the saturation field using the quasi-global mixed MsFEM and the saturation field using the local mixed MsFEM, respectively. Here 10×10 coarse grid is taken for both the quasi-global mixed MsFEM and the local mixed MsFEM and the viscosity ratio is $\mu_w/\mu_o = 1/10$. In the quasi-global mixed MsFEM, the homogenized velocity u_δ^* is taken to construct boundary conditions for the basis functions. The corresponding relative saturation error and water-cut curve are shown in Figure 4. More detailed numerical comparisons are presented in Tables 1 and 2, where the grid size for k_δ is fixed at 50×50 and different coarse grids are used for the mixed MsFEM implementation. From Tables 1 and 2, we can observe: (1) the quasi-global mixed MsFEM provides several times better accuracy than the local mixed MsFEM; (2) as the coarse grid size decreases, errors also decrease.

Table 1: Relative Errors (k_δ defined on 50×50 grid, $\frac{\mu_w}{\mu_0} = 1/10$)

Coarse Grid	Water-Cut Error Q.-Glob. MsFEM	Saturation Error Q.-Glob. MsFEM	Water-Cut Error Local MsFEM	Saturation Error Local MsFEM
10×10	0.0051	0.0511	0.1164	0.2497
20×20	0.0019	0.0249	0.0996	0.2005
30×30	0.0018	0.0185	0.0557	0.1094
60×60	0.0008	0.0095	0.0164	0.0434

Table 2: Relative Errors (k_δ defined on 50×50 grid, $\frac{\mu_w}{\mu_0} = 1/3$)

Coarse Grid	Water-Cut Error Q.-Glob. MsFEM	Saturation Error Q.-Glob. MsFEM	Water-Cut Error Local MsFEM	Saturation Error Local MsFEM
10×10	0.0101	0.0473	0.1595	0.2451
20×20	0.0042	0.0241	0.1359	0.1972
30×30	0.0031	0.0170	0.0788	0.1115
60×60	0.0014	0.0096	0.0219	0.0430

In our next numerical example, the permeability field (SPE 10, layer 60) is interpolated to 220×220 fine grid. Various coarse grids are used in two-phase flow simulations without updating basis functions in the numerical experiments. We depict the fine-scale SPE 10 permeability and 55×55 upscaled permeability in Figure 5. Figure 6 depicts the fine-scale saturation, the saturation using the quasi-global mixed MsFEM and the saturation using the local mixed MsFEM, respectively, where 11×11 coarse grid is taken for the mixed MsFEM and the viscosity ratio is $\mu_w/\mu_o = 1/10$. Here 55×55 grid is taken for upscaling to produce the upscaled velocity that is used to construct boundary conditions of the basis functions. The corresponding relative saturation error and water-cut curve are shown in Figure 7. We observe that the use of approximate global information in the mixed MsFEM reduces the error about 2 times compared to purely local methods. Table 3 shows the numerical errors for different coarse grids. As we observe from this table that as the coarse-grid size decreases,

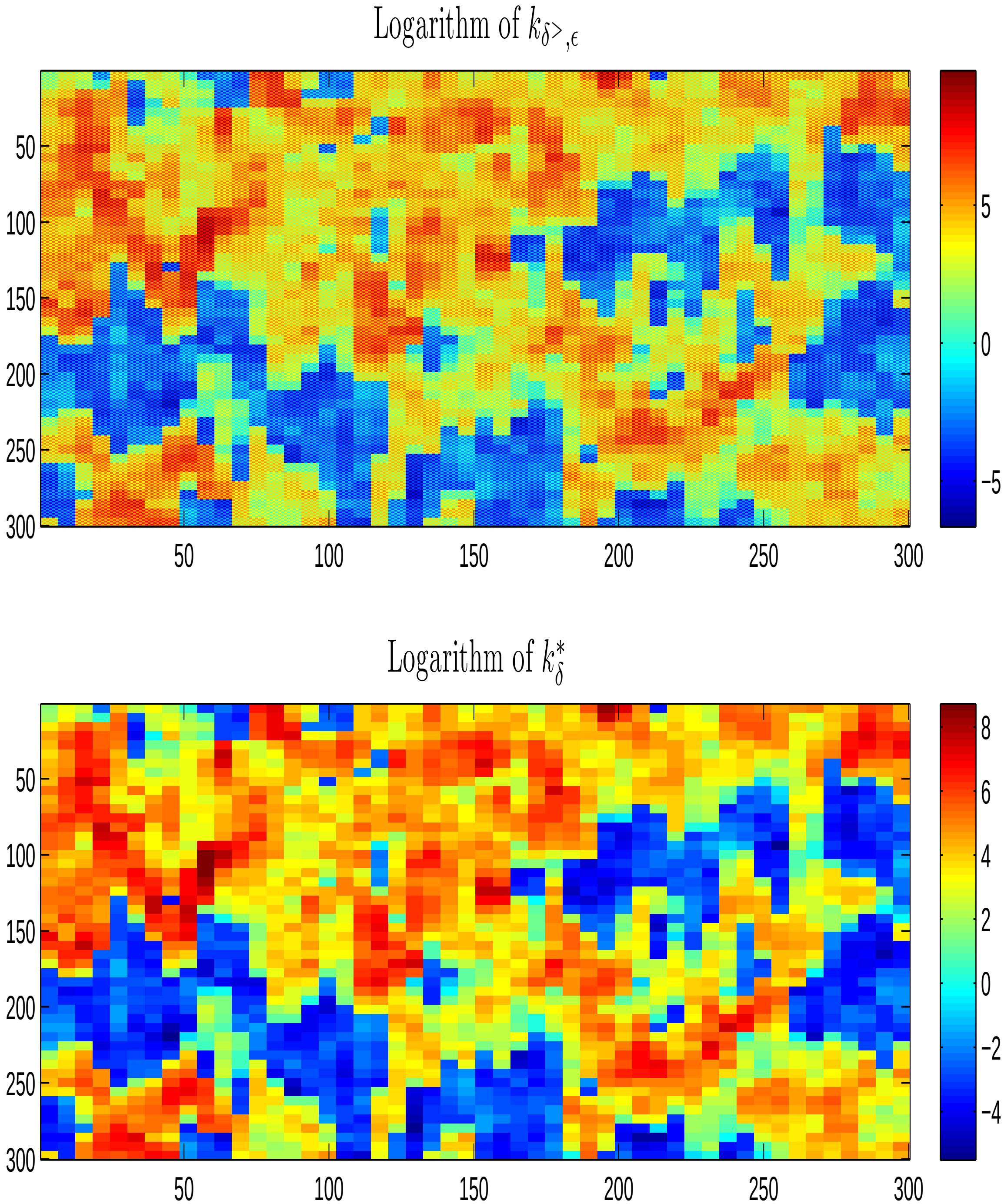

Figure 2: Top: Logarithm of $k_{\delta>,\epsilon}$ permeability. Bottom: Logarithm of homogenized permeability k_δ^* .

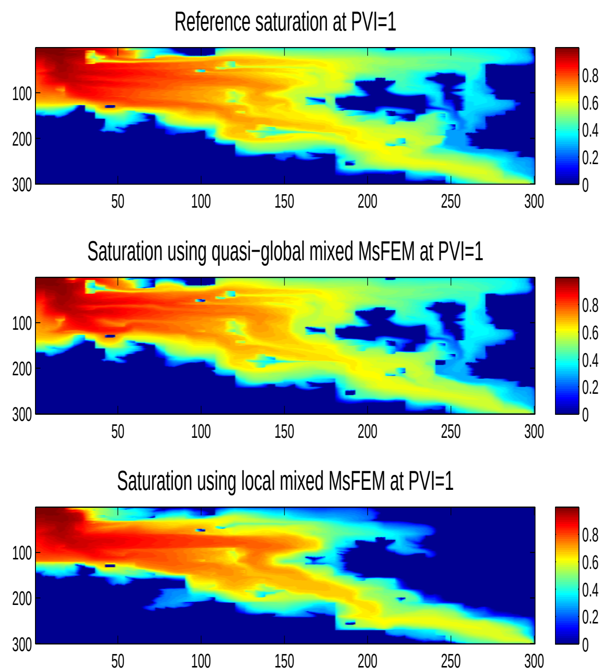

Figure 3: Top: Reference saturation at PVI=1 $\mu_w/\mu_0 = 1/10$, permeability $k_{\delta>,\epsilon}$. Middle: Saturation at PVI=1 by the quasi-global mixed MsFEM. Bottom: Saturation at PVI=1 by the local mixed MsFEM.

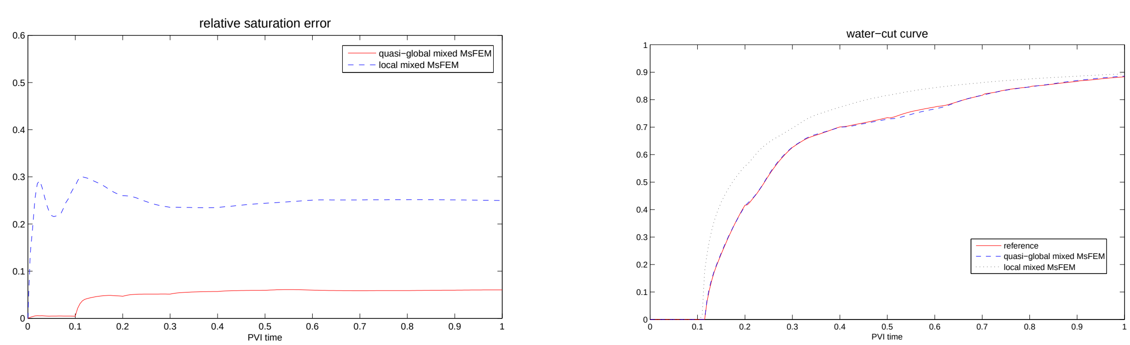

Figure 4: The saturation error (left) and water-cut curve (right), permeability $k_{\delta>,\epsilon}$, $\mu_w/\mu_0 = 1/10$.

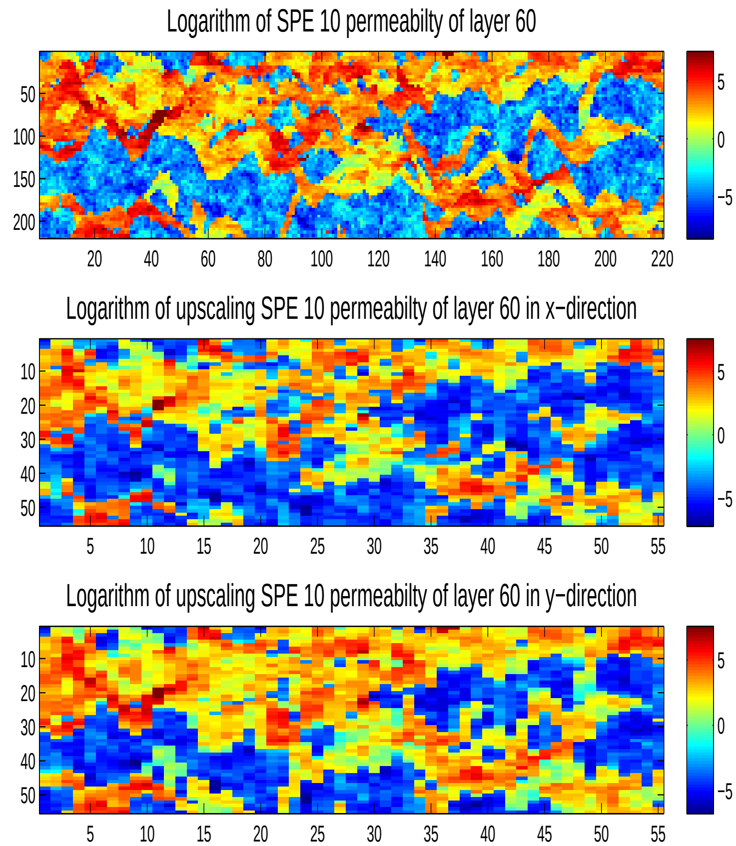

Figure 5: Top: Logarithm of SPE 10 fine-scale permeability (layer 60). Middle: Logarithm of upscaling the SPE 10 fine-scale permeability (layer 60) in x-direction (55×55). Bottom: Logarithm of upscaling the SPE 10 fine-scale permeability (layer 60) in y-direction (55×55).

the error also decreases. Note that this is not the case when purely local methods are used (see Table 3). In Table 4, we show the numerical errors when the coarse grid for the mixed MsFEM is fixed and different upscaling grids are used for the construction of boundary conditions of multiscale basis functions. We note from this table that the error decreases as the upscaling grid becomes finer. Indeed, as we refine the upscaling grid, more precise global information is passed to the multiscale basis functions. This improves the accuracy of the method. The water-cut as well as saturation errors are depicted in Figure 8. We note that if the coarse grid is the same as upscaling grid, then the quasi-global mixed MsFEM reduces to the local mixed MsFEM. This result is illustrated at the intersection point (in Figure 8) of the red solid line (local mixed MsFEM) and the blue dashed line (quasi-global mixed MsFEM), where the upscaling grid and the coarse grid are the same, i.e., 11×11. If the upscaling grid is taken to be the fine grid, then the quasi-global mixed MsFEM becomes the global mixed MsFEM as proposed in [2].

For our next simulation results, we choose a realization of the permeability field generated

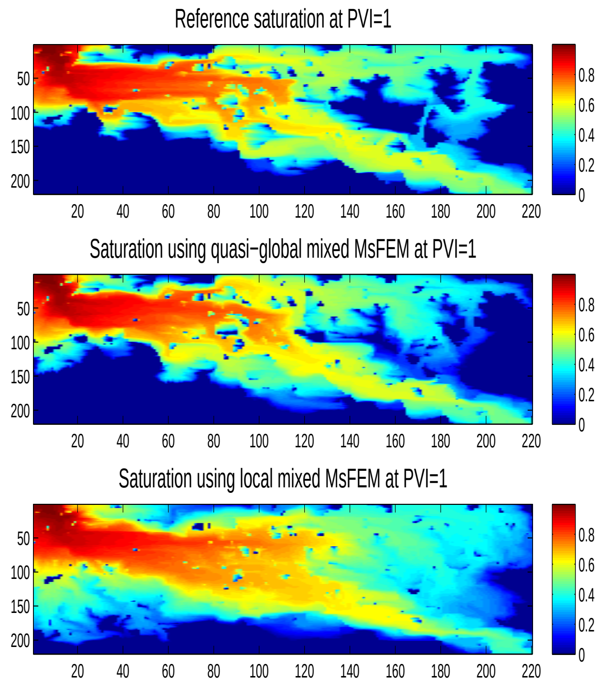

Figure 6: Top: Reference saturation at PVI=1 $\mu_w/\mu_0 = 1/10$, SPE 10 permeability. Middle: Saturation at PVI=1 by the quasi-global mixed MsFEM. Bottom: Saturation at PVI=1 by the local mixed MsFEM.

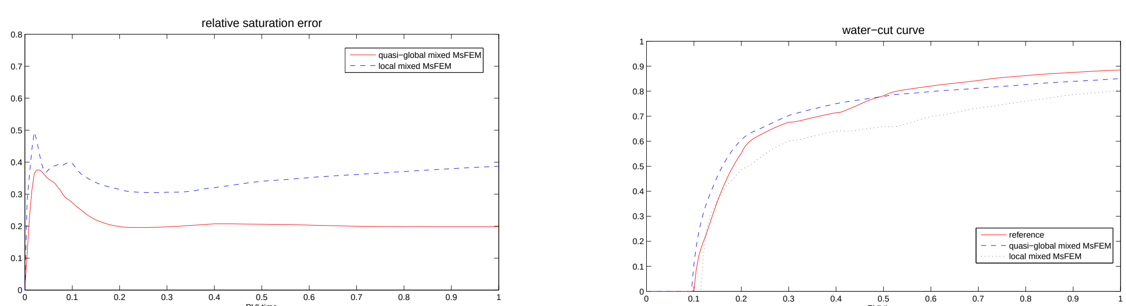

Figure 7: The saturation error (left) and water-cut curve (right), SPE 10 permeability, $\mu_w/\mu_0 = 1/10$.

Table 3: Relative Errors (55×55 upscaling grid, $\frac{\mu_w}{\mu_0} = 1/10$)

Coarse Grid	Water-Cut Error Q.-Glob. MsFEM	Saturation Error Q.-Glob. MsFEM	Water-Cut Error Local MsFEM	Saturation Error Local MsFEM
5×5	0.1260	0.4057	0.1982	0.4086
10×10	0.0853	0.2704	0.1177	0.3426
22×22	0.0482	0.2240	0.1053	0.3644

Table 4: Relative Errors (11 × 11 coarse grid, $\frac{\mu_w}{\mu_0} = 1/10$)

Upscaling Grid	Water-Cut Error Q.-Glob. MsFEM	Saturation Error Q.-Glob. MsFEM
11 × 11	0.1302	0.3549
22 × 22	0.0977	0.3019
55 × 55	0.0562	0.2145
110 × 110	0.0355	0.1219
220 × 220	0.0032	0.0650

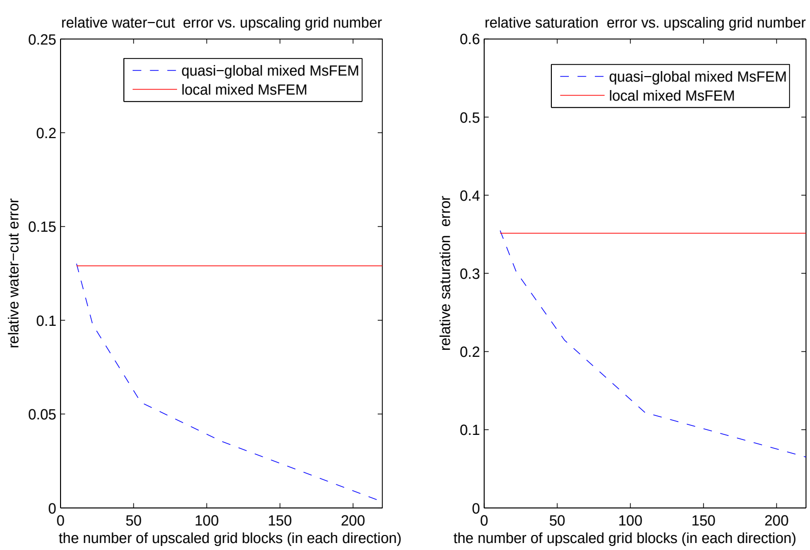

Figure 8: Water-cut error and saturation error vs. different upscaling grids.

using a two-point correlation function with correlation lengths in x_1-direction $L_1 = 0.4$ and in x_2-direction $L_2 = 0.05$. Exponential variogram is selected (see e.g., [15]). We depict 200×200 fine-grid permeability field and 40×40 upscaled permeability in Figure 9. Figure 10 depicts the fine-scale saturation, the saturation using the quasi-global mixed MsFEM and the saturation using the local mixed MsFEM, respectively, where 10×10 coarse grid is taken for both the quasi-global mixed MsFEM and the local mixed MsFEM and the viscosity ratio is $\mu_w/\mu_o = 1/3$. In the quasi-global mixed MsFEM, 40×40 coarse grid is taken for the upscaling of the permeability field to produce the upscaled velocity, which is used to construct boundary conditions for multiscale basis functions. The corresponding relative saturation errors and water-cut curves at different times are plotted in Figure 11. First, we note that the errors due to MsFEMs are smaller compared to the cases when SPE 10 permeability fields are used. The errors due to the local mixed MsFEM in the saturation field are about 5 % at $PVI > 0.5$. We observe that the mixed MsFEM using approximate global information produces errors which are lower consistently over the time. These errors are are shown in Tables 5 and 6 for different viscosity ratios. We observe from these tables that the quasi-global mixed MsFEM provides better accuracy compared to the local mixed MsFEM. Moreover, as the coarse-grid size decreases, the errors due to the quasi-global mixed MsFEM decreases, while the errors for the local mixed MsFEM do not change on average. In Table 7, we fix the coarse-grid size and change the upscaling grid. We can observe from this table that as the intermediate coarse-grid size (that is used for the upscaling) decreases, the quasi-global mixed MsFEM becomes more accurate. As we noted earlier, when the upscaling grid becomes finer, the global information is more accurate. Consequently, the mixed MsFEM using approximate global information becomes more accurate.

Table 5: Relative Errors (40×40 upscaling grid, $\frac{\mu_w}{\mu_0} = 1/10$)

Coarse Grid	Water-Cut error Q.-Glob. MsFEM	Saturation Error Q.-Glob. MsFEM	Water-Cut Error Local MsFEM	Saturation Error Local MsFEM
8×8	0.0137	0.0166	0.0229	0.0397
10×10	0.0124	0.0136	0.0203	0.0485
20×20	0.0060	0.0107	0.0222	0.0243

Table 6: Relative Errors (40×40 upscaling grid, $\frac{\mu_w}{\mu_0} = 1/3$)

Coarse Grid	Water-Cut Error Q.-Glob. MsFEM	Saturation Error Q.-Glob. MsFEM	Water-Cut Error Local MsFEM	Saturation Error Local MsFEM
8×8	0.0353	0.0195	0.0414	0.0457
10×10	0.0269	0.0158	0.0467	0.0579
20×20	0.0093	0.0117	0.0377	0.0254

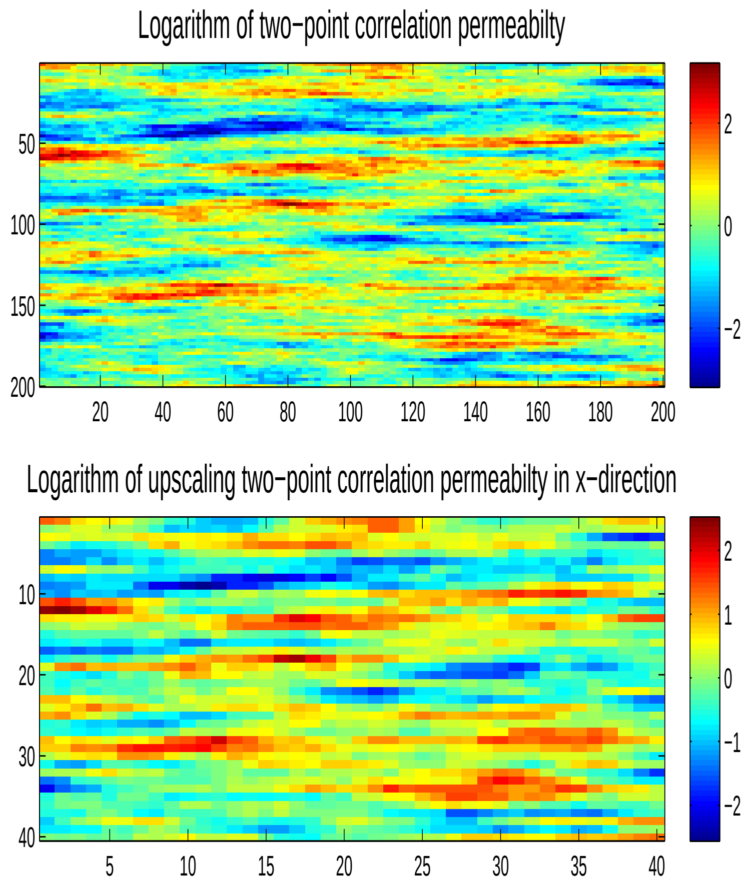

Figure 9: Top: Logarithm of two-point correlation permeability with $L_x = 0.4$ and $L_y = 0.05$. Bottom: Logarithm of upscaling the two-point correlation permeability in x-direction.

Table 7: Relative Errors (10×10 coarse grid, $\frac{\mu_w}{\mu_0} = 1/10$)

Upscaling Grid	Water-Cut Error Q.-Glob. MsFEM	Saturation Error Q.-Glob. MsFEM
10 × 10	0.0191	0.0491
20 × 20	0.0170	0.0209
40 × 40	0.0124	0.0136
50 × 50	0.0122	0.0129

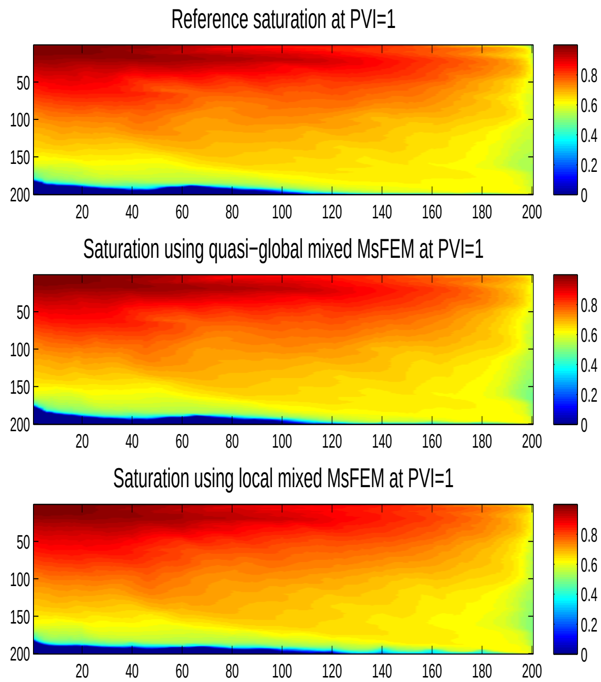

Figure 10: Top: Reference saturation at PVI=1 $\mu_w/\mu_0 = 1/3$, two-point correlation permeability. Middle: Saturation at PVI=1 by the quasi-global mixed MsFEM. Bottom: Saturation at PVI=1 by the local mixed MsFEM.

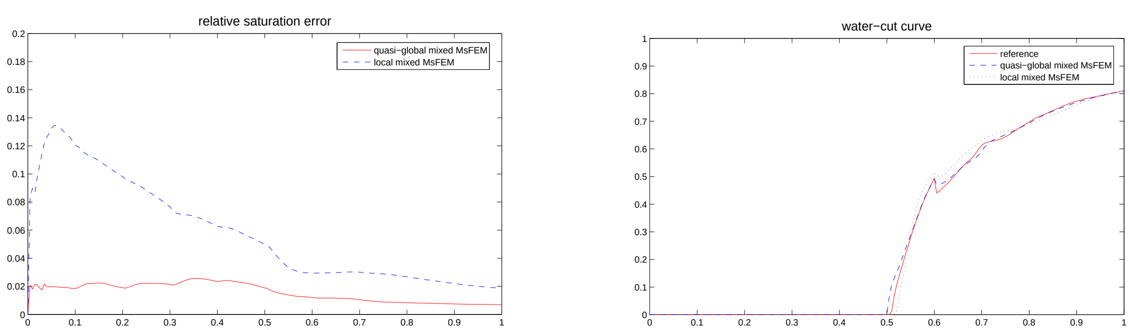

Figure 11: The saturation error (left) and water-cut curve (right), two-point correlation permeability, $\mu_w/\mu_0 = 1/3$.

5 Conclusions

In this paper, we study the use of approximate global information in multiscale simulations. Previous approaches involve fine-scale simulations in the computation of the global information. In these cases, the computation of global fields can be expensive. In this paper, we propose the use of partial homogenization in constructing approximate global fields. The main idea of this approach is to upscale the media properties to some intermediate coarse grid that is larger than the fine-mesh size, while it is finer than the target coarse-grid block. The objective is to homogenize the small scales whose effects can be captured with multiscale basis functions. The use of non-uniform coarsening will further help to reduce the degrees of freedoms involved in the computation of approximate global fields. We present mathematical analysis of the method by introducing a formalism for having both separable and non-separable scales in the coefficients. The proposed method is applied to simulate two-phase flows in heterogeneous porous media. Numerical results are presented for various permeability fields including those generated using two-point correlation functions and channelized permeability fields from SPE Comparative Project [14]. We consider simple cases where one can identify the scales which can be homogenized. For more general cases, we suggest the use of upscaling on the coarse grid with the size smaller than the target coarse grid where multiscale basis functions are constructed. This intermediate coarse grid renders a partially homogenized solution that contains essential non-local information. Numerical examples demonstrate that the use of approximate global information provides better accuracy than purely local multiscale methods.

6 Acknowledgments

We are very grateful to Jorg Aarnes for providing mixed MsFEM codes. YE would like to acknowledge a partial support from NSF and DOE. YE's work was also partially supported by Award Number KUS-CI-016-04, made by King Abdullah University of Science and Technology (KAUST).

References

[1] J. Aarnes, *On the use of a mixed multiscale finite element method for greater flexibility and increased speed or improved accuracy in reservoir simulation*, SIAM MMS, 2 (2004), pp. 421–439.

[2] J. Aarnes, Y. Efendiev and L. Jiang, *Mixed multiscale finite element methods using limited global information*, SIAM, Multiscale Modeling and Simulation, 7 (2) (2008), pp. 655–676.

[3] J.E. Aarnes, V. Hauge, and Y. Efendiev. *Coarsening of three-dimensional structured and unstructured grids for subsurface flow.* Advances in Water Resources, 30(11) (2007), pp. 2177-2193.

[4] G. Allaire and R. Brizzi, A multiscale finite element method for numerical homogenization, SIAM MMS, 4(3) (2005), pp. 790–812.

[5] T. Arbogast, *Implementation of a locally conservative numerical subgrid upscaling scheme for two-phase Darcy flow*, Comput. Geosci., 6 (2002), pp. 453–481.

[6] T. Arbogast, G. Pencheva, M. F. Wheeler, and I. Yotov, *A multiscale mortar mixed finite element method*, SIAM J. Multiscale Modeling and Simulation, 6 (2007), pp. 319-346.

[7] M. Avellaneda and F.-H. Lin, *Compactness method in the theory of homogenization*, Comm. Pure Appl. Math. 40 (6) (1987), pp. 803–847.

[8] I. Babuška, G. Caloz, and E. Osborn, *Special finite element methods for a class of second order elliptic problems with rough coefficients*, SIAM J. Numer. Anal., 31 (1994), pp. 945–981.

[9] I. Babuška and E. Osborn, *Generalized finite element methods: Their performance and their relation to mixed methods*, SIAM J. Numer. Anal., 20 (1983), pp. 510–536.

[10] F. Brezzi, *Interacting with the subgrid world*, in Numerical analysis 1999 (Dundee), Chapman & Hall/CRC, Boca Raton, FL, 2000, pp. 69–82.

[11] F. Brezzi and M. Fortin , *Mixed and hybrid finite element methods*, Springer–Verlag, Berlin – Heidelberg – New-York, 1991.

[12] Y. Chen, L. J. Durlofsky, M. Gerritsen, and X. H. Wen, *A coupled local-global upscaling approach for simulating flow in highly heterogeneous formations*, Advances in Water Resources, 26 (2003), pp. 1041–1060.

[13] Z. Chen and T. Y. Hou, *A mixed multiscale finite element method for elliptic problems with oscillating coefficients*, Math. Comp., 72 (2002), pp. 541–576.

[14] M. Christie and M. Blunt, *Tenth SPE Comparative Solution Project: A comparison of upscaling techniques*, SPE Reser. Eval. Eng., 4 (2001), pp. 308–317.

[15] C. Deutsch and A. Journel, *GSLIB: Geostatistical software library and user's guide, 2nd edition*, Oxford University Press, New York, 1998.

[16] L.J. Durlofsky, *Numerical calculation of equivalent grid block permeability tensors for heterogeneous porous media.* Water Resour. Res., 27 (1991), pp. 699–708.

[17] L.J. Durlofsky, Y. Efendiev, and V. Ginting. *An adaptive local-global multiscale finite volume element method for two-phase flow simulations.* Advances in Water Resources, 30:576–588, 2007.

[18] Y. Efendiev, V. Ginting, T. Hou, and R. Ewing, *Accurate multiscale finite element methods for two-phase flow simulations*, J. Comp. Physics., 220 (1), pp. 155–174, 2006.

[19] Y. Efendiev, T. Hou, and V. Ginting, *Multiscale finite element methods for nonlinear problems and their applications*, Comm. Math. Sci., 2 (2004), pp. 553–589.

[20] L.C. Evans, *Partial differential equations*, American Mathematical Society, 1998.

[21] L. Franca, A. Madureira, and F. Valentin, *Towards multiscale functions: Enriching finite element spaces with local but not bubble-like functions.* Comput. Meth. Appl. Mech. Eng., 194(27–29):3006–3021, 2005.

[22] T. Y. Hou and X. H. Wu, *A multiscale finite element method for elliptic problems in composite materials and porous media*, Journal of Computational Physics, 134 (1997), pp. 169–189.

[23] T. Hughes, G. Feijoo, L. Mazzei, and J. Quincy, *The variational multiscale method - a paradigm for computational mechanics*, Comput. Methods Appl. Mech. Engrg, 166 (1998), pp. 3–24.

[24] P. Jenny, S. H. Lee, and H. Tchelepi, *Multi-scale finite volume method for elliptic problems in subsurface flow simulation*, J. Comput. Phys., 187 (2003), pp. 47–67.

[25] ——, *Adaptive multi-scale finite volume method for multi-phase flow and transport in porous media*, Multiscale Modeling and Simulation, 3 (2005), pp. 30–64.

[26] V. Jikov, S. Kozlov, and O. Oleinik, *Homogenization of differential operators and integral functionals,* Springer-Verlag, 1994, Translated from Russian.

[27] A.-M. Matache and C. Schwab, *Homogenization via p-FEM for problems with microstructure*, in Proceedings of the Fourth International Conference on Spectral and High Order Methods (ICOSAHOM 1998) (Herzliya), vol. 33, 2000, pp. 43–59.

[28] S. Moskow and M. Vogelius, *First-order corrections to the homogenised eigenvalues of a periodic composite medium. A convergence proof*, Proc. Roy. Soc. Edinburgh Sect. A 127 (6) (1997), pp. 1263–1299.

[29] F. Murat and L. Tartar, *H-convergence, in topics in the mathematical modeling of composite materials, A. Cherkaev and R.V. Kohn eds.series: Progress in Nonlinear Differential equations and their Applications*, Birkhauser, Boston 1997

[30] H. Owhadi and L. Zhang, *Metric based up-scaling*, Comm. Pure Appl. Math., 60 (2007), pp. 675–723.

[31] G. Sangalli, *Capturing small scales in elliptic problems using a residual-free bubbles finite element method*, Multiscale Model. Simul., 1 (2003), pp. 485–503 (electronic).

[32] X.H. Wu, Y. Efendiev, and T.Y. Hou, *Analysis of upscaling absolute permeability*, Discrete and Continuous Dynamical Systems, Series B 2 (2) (2002), pp. 185–204.